

Supplementary Information

High-Performance Supercapacitors: Electrochemical Insights into CoP/MXene Nanomaterial Performance

Palanisamy Rajkumar ^a, Vedyappan Thirumal ^a, Md. Masud Rana ^b, Wei Xiao ^a, Joongpyo Shim ^{b,*},
Kisoo Yoo ^{a,*}, Jinho Kim ^{a,*}

^a Department of Mechanical Engineering, Yeungnam University, Gyeongsan-si, Gyeongbuk-do 38541, Republic of Korea

^b Department of Chemical Engineering, Kunsan National University, Jeonbuk, 54150, South Korea

Corresponding authors: jinho@ynu.ac.kr (JK); kisoo@ynu.ac.kr (KY); jpshim@kunsan.ac.kr (JS)

Preparation of MXene:

For the preparation of MXene, initially 2g of the MAX phase (Ti_3AlC_2) was etched with 60 mL of Hydrofluoric acid (HF, 48%) by continuously stirring for 5. Subsequently, 200 mL of deionized water was added to the solution and washed multiple times to maintain a neutral pH. Later, 40 mL of Dimethyl Sulfoxide (DMSO) was introduced for the intercalation and delamination process of the MXene solution and was stirred for 15 minutes, followed by centrifugation to obtain a black suspension. Lastly, the solution was filtered and dried in an oven at 60 °C overnight to yield the final product.

Device fabrication:

The active materials (CoP, CoP/MXene), polyvinylidene fluoride (PVdF), and Super P are combined in an 80:10:10 ratio and ground into a slurry, incorporating N-methyl-2-pyrrolidone (NMP). This slurry is then coated onto Ni-foam with dimensions of 2 cm × 1 cm and dried at 60 °C in a hot air oven.

The fabrication of the asymmetric supercapacitor device involves sealing the Ni-foam coated with the active material (positive electrode) and another Ni-foam coated with activated carbon (AC) (negative electrode). These electrodes are separated by Whatman filter paper immersed in a KOH solution, forming a pouch cell.

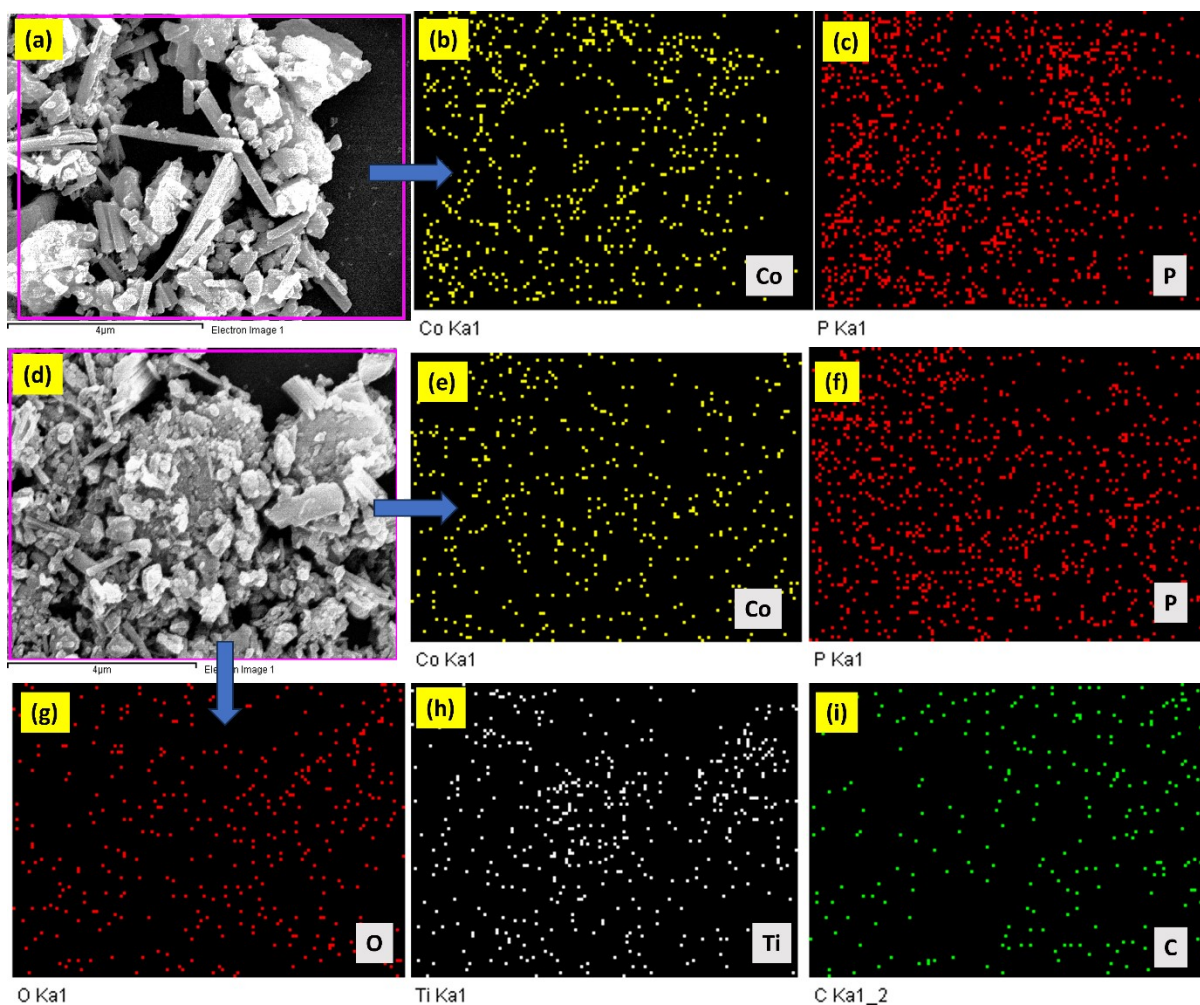


Figure S1: FESEM image of CoP (a), CoP/MXene (d); elemental mapping of CoP (b,c) and CoP/MXene (e – i).

The elemental mapping of CoP and CoP/MXene shows uniform distribution of elements in the prepared samples.

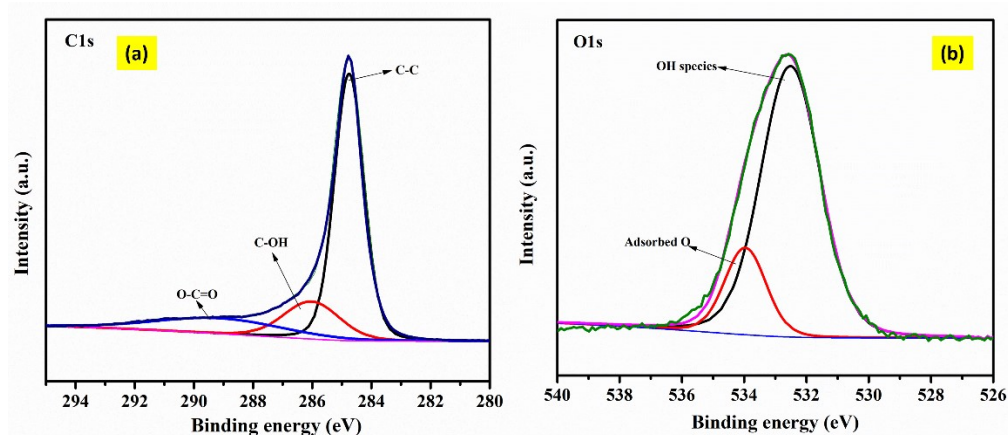
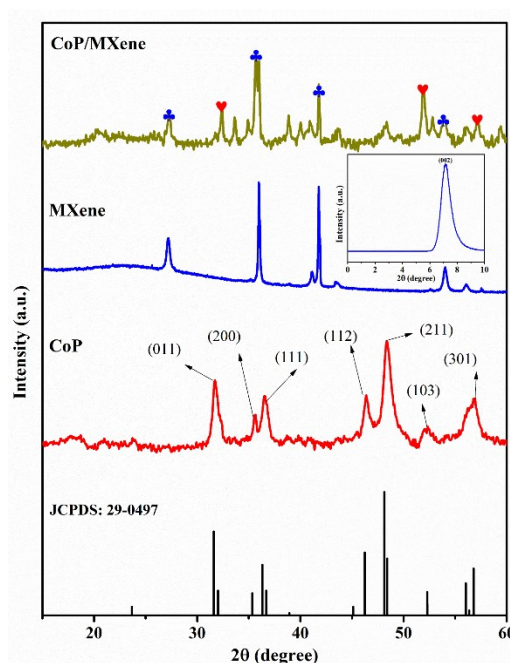


Figure S2: Deconvoluted spectra of C 1s (a) and O 1s (b).

Table S1: Binding energy and the corresponding elemental states.

Elements	Binding energy (eV)	Elemental State
Ti 2p	465	TiO ₂
	459	Ti – C
O 1s	533	Absorbed O
	532	OH Species
C 1s	289	O – C = O
	286	C – OH
	284	C – C

**Figure S3:** XRD spectra of CoP, MXene (Inset: Spectra from 0 to 10°) and CoP/MXene

The prepared CoP aligns well with the JCPDS no: 29-0497. The XRD pattern exhibits distinct peaks at 2θ values of 31.7° , 35.2° , 36.5° , 46.4° , 48.5° , 52.4° , and 57° , corresponding to the (011), (200), (111), (112), (211), (103), and (301) diffraction planes, respectively. In the XRD plot of MXene, discernible peaks are observed at 27.2° , 36° , and 41.9° , aligning with the (101), (103), and (105) diffraction planes. Notably, the characteristic Al peak from the precursor Ti_3AlC_2 is significantly diminished. The XRD plot of the CoP/MXene composite reveals combined peaks from both CoP and MXene, as indicated in Figure S3(a). The composite's XRD pattern is indicative of the coexistence of the crystalline phases of CoP and MXene within the synthesized material.

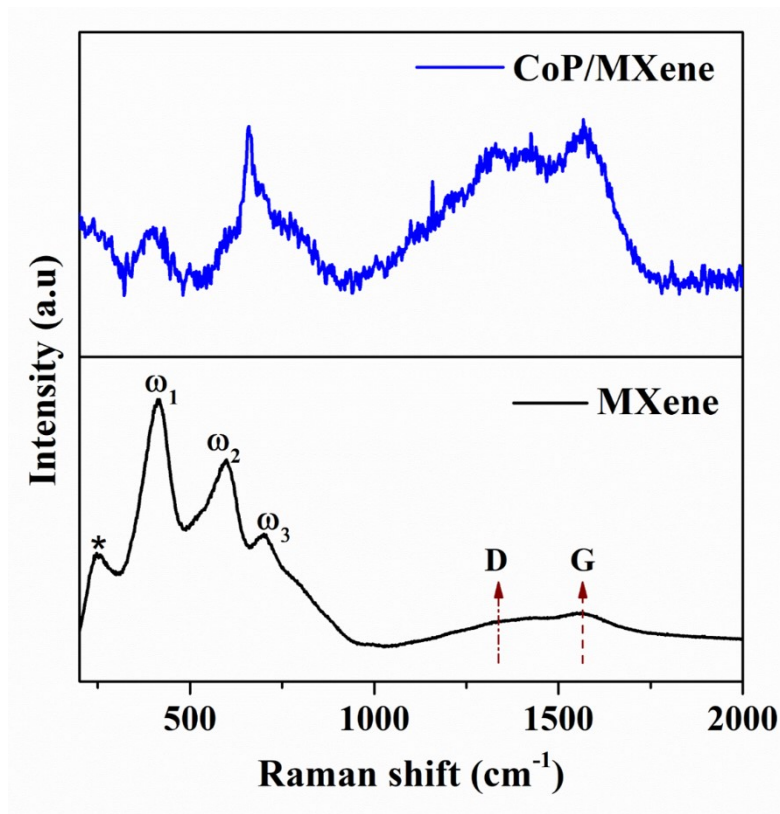


Figure S4: Raman spectra of CoP, MXene and CoP/MXene

The Raman peaks of MXene exhibit D and G bands, which are attributed to sp^2 carbon sites. These bands are indicative of disordered and graphitic carbon structures in the material. The presence of the G band is associated with carbon-carbon bonding, while the D band signifies perturbed sp^2 carbon rings. A distinct peak at 244 cm^{-1} (marked as *) in the Raman spectra can be attributed to out-of-plane vibrations of titanium (Ti) and carbon (C) atoms within the material. These observed Raman features are consistent with findings reported in the literature [S1].

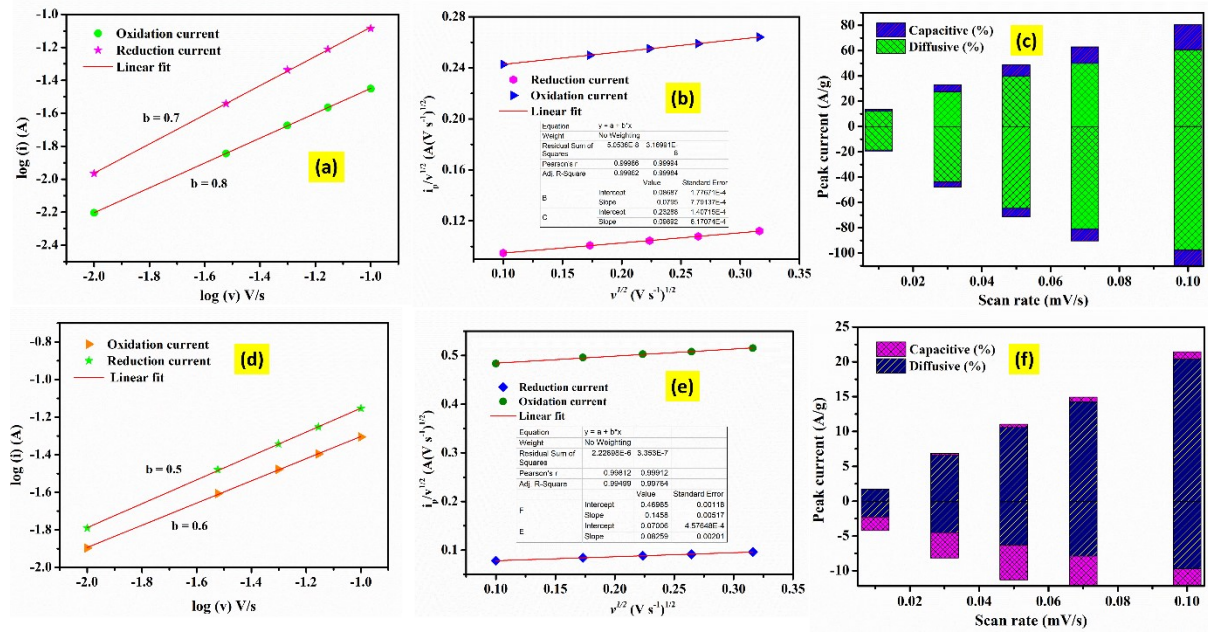


Figure S5: b value calculation, plot between $i_p/v^{1/2}$ and $v^{1/2}$ and bar-diagram depicting capacitive and diffusive behavior of: CoP (a – c); CoP/MXene (d – f).

The sequential reduction and oxidation reactions of OH^- ions with BSO-based electrodes can be analysed through a power-law model, as presented below:

$$i_p = a \times v^b \quad (\text{Eq. S1})$$

Here, i_p represents the peak current (A), v denotes the scan rate (V/s), a represents a constant, and b implies the exponent. The power law is utilized to determine the b value, as indicated by the slope of the linear fit for $\log(v)$ versus $\log(i)$ as shown in figure S4(c, d). The Modified Power Law is utilized to examine the diffusion and capacitive-controlled reactions taking place at the electrode/electrolyte interface. The equation is provided below:

$$i_p = k_1 v + k_2 v^{1/2} \quad (\text{Eq. S2})$$

$$i_p/v^{1/2} = k_1 v^{1/2} + k_2 \quad (\text{Eq.S3})$$

The summation of the equation gives rise to both the diffusion-controlled process ($k_2 v^{1/2}$) and the capacitive-controlled process ($k_1 v$), collectively influencing the peak current (i_p). Figure S4 (b, e) illustrates the correlation between the square root of the scan rate ($v^{1/2}$) and

the ratio of peak current to scan rate ($i_p/v^{1/2}$). The slope and intercept extracted from this plot were employed to ascertain the capacitive and diffusive behavior of the CoP and CoP/MXene electrode. For both the CoP electrode (95% anodic, 91% cathodic) and CoP/MXene (97% anodic, 92% cathodic), at a scan rate of 10 mV s⁻¹, the anodic and cathodic peaks demonstrated a diffusion-controlled process, contributing to most of the observed behaviour.

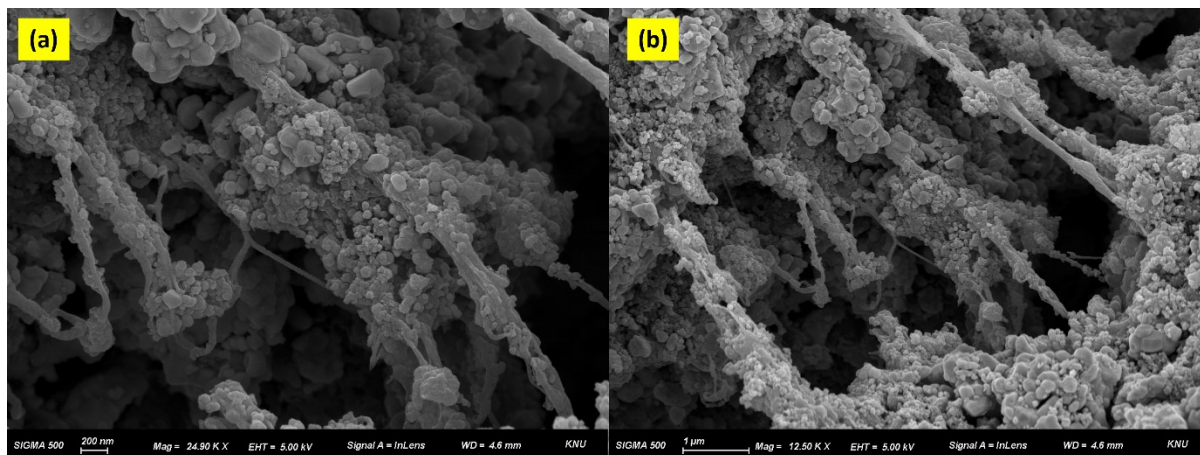


Figure S6: SEM image of cycled CoP/MXene electrode.

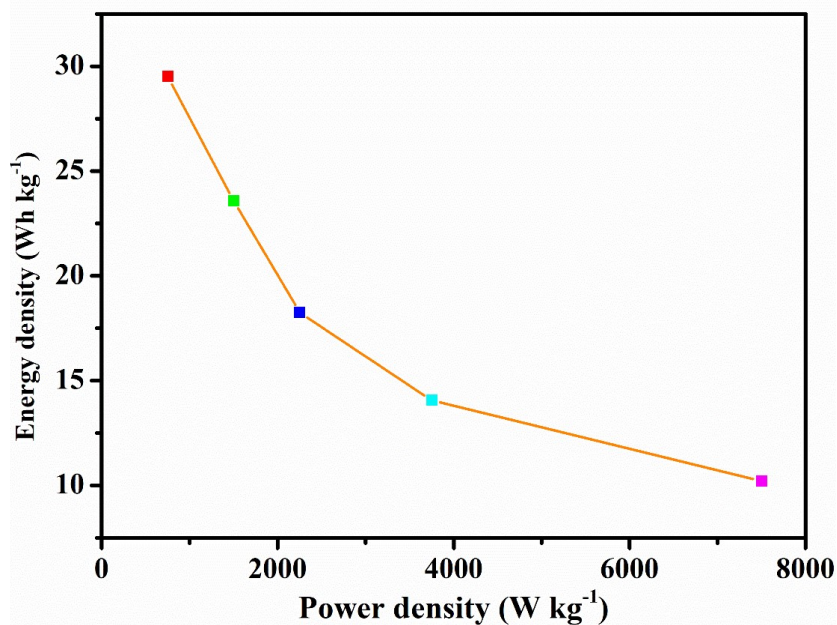


Figure S7: Power density Vs Energy density of CoP/MXene || AC ASC device.

Sl.No:	Material	Capacitance (F g ⁻¹)	Ref
1.	NiMX ₂	474.3	[S2]
2.	COF/MXene	390	[S3]
3.	MXene/Graphene/NiO	558.788	[S4]

4.	CNT@NiCoAl-LDH@MXene	179	[S5]
5.	porous MXene film	223.4	[S6]
6.	N – Ti ₃ C ₂ T _x	449	[S7]

References:

- [S1] I. Anum, N.M. Hamdan, *Materials*, 2021, 14(21), 6292.
- [S2] Nanda, Om Priya, Aksha Gilbert Prince, Lignesh Durai, and Sushmee Badhulika. *Energy & Fuels*, 2023, 37(6) 4701-4710.
- [S3] An, Ning, Zhen Guo, Chao Guo, Maoqing Wei, Daming Sun, Yuanyuan He, Wenli Li, Lei Zhou, Zhongai Hu, and Xiuyan Dong, *Chemical Engineering Journal*, 2023, 458, 141434.
- [S4] Sarwar, Sakhi G., Imosobomeh L. Ikhioya, Shahbaz Afzal, and Ishaq Ahmad, *Hybrid Advances*, 2023, 4, 100105.
- [S5] Zhang, Le, Yue Wang, Yanmeng Cai, Rongli Fang, Shunjiang Huang, Yanshuang Zhao, and Shasha Zhang, *Chemical Engineering Journal*, 2023, 478, 147270.
- [S6] Yan, Sai, Chenjing Shi, Zhen Tian, Dan Li, Yanjun Chen, Li Guo, and Yanzhong Wang, *Chemical Engineering Journal*, 2023, 478, 147393.
- [S7] Cai, Man, Xiaochun Wei, Haifu Huang, Fulin Yuan, Cong Li, Shuaikai Xu, Xianqing Liang, Wenzheng Zhou, and Jin Guo, *Chemical Engineering Journal*, 2023, 458, 141338.